Facile preparation of hydrated vanadium pentoxide nanobelts based bulky paper as flexible binder-free cathodes for high-performance lithium ion batteries

Rui, Xianhong; Zhu, Jixin; Liu, Weiling; Tan, Huiteng; Sim, Daohao; Xu, Chen; Zhang, Hua; Ma, Jan; Hng, Huey Hoon; Yan, Qingyu; Lim, Tuti Mariana

2011

Rui, X., Zhu, J., Liu, W., Tan, H., Sim, D., Xu, C., et al. (2011). Facile preparation of hydrated vanadium pentoxide nanobelts based bulky paper as flexible binder-free cathodes for high-performance lithium ion batteries. RSC Advances, 1, 117-122.

https://hdl.handle.net/10356/95034

https://doi.org/10.1039/c1ra00281c

RSC Advances

Dynamic Article Links

Cite this: DOI: 10.1039/c0xx00000x

www.rsc.org/xxxxxx

ARTICLE TYPE

Facile preparation of hydrated vanadium pentoxide nanobelts based bulky paper as flexible binder-free cathodes for high-performance lithium ion batteries†

Xianhong Rui,[ab] Jixin Zhu,[a] Weiling Liu,[a] Huiteng Tan,[a] Daohao Sim,[a] Chen Xu,[a] Hua Zhang,[a] Jan Ma,[a] Huey Hoon Hng,[a] Tuti Mariana Lim*[bd] and Qingyu Yan*[ace]

Received (in XXX, XXX) Xth XXXXXXXXX 20XX, Accepted Xth XXXXXXXXX 20XX
DOI: 10.1039/b000000x

Hydrated vanadium pentoxide ($V_2O_5{\cdot}0.44H_2O$, HVO) nanobelts were synthesized by a simply high-yield (*e.g.* up to ~99%) hydrothermal approach. The length of these nanobelts was up to several hundred micrometers while the diameter was only ~20 nm and the thickness was ~10 nm. Binder-free bulky papers were prepared by using these HVO nanobelts and were tested as Li ion battery cathodes. The unique architecture of the HVO bulky paper provides hierarchical porous channels and large specific surface area, which facilitate fast ion diffusion and effectively strain relaxation upon charge-discharge cycling. The electrochemical tests revealed that the flexible HVO cathode could deliver high reversible specific capacities with ~100% Coulombic efficiency, especially at high C rates. For example, it achieved a reversible capacity of 163 mAh g^{-1} at 6.8 C.

Introduction

Nowadays, there are rapid growing demands for portable electronic devices with various specifications, *e.g.* low-cost, paper-thin, lightweight, flexible and even rollable. Therefore the development of power sources, such as rechargeable Li-ion batteries, is desired to further improve their power and energy density, operational safety, cycling stability and even flexibility (working well even under twisting conditions). For traditional Li-ion battery electrodes, polymer binders or adhesives are added to improve the binding of active materials to substrates, which, however, also causes an undesirable decrease in the film's electrical conductivity. Binder-free electrodes also open up a possibility for high temperature applications in excess of 200 °C, at which most conventional binders are not stable.[1] Currently, binder-free and bulky-paper-formed flexible electrodes were prepared by using carbon based materials, including carbon nanotubes (CNTs)[2] and graphene nanosheets.[3] However, their applications are limited to Li-ion battery anodes. In addition, there are concerns that the cost of CNTs is high and the preparation of graphene sheets is tedious. Hence there is a need to search for other flexible active materials with good electrochemical performance and low-cost especially for cathode applications.

Vanadium pentoxide (V_2O_5) has been extensively studied as a well-known cathode material for Li-ion batteries owning to its essential advantages of low cost, easy synthesis process, high safety, high specific capacity and energy density.[4–6] It is a typical intercalation compound with a layered crystal structure, which can act as a good host for the reversible insertion and extraction of Li^+ and can attain a large theoretical capacity of 294 mAh g^{-1} in the voltage range of 4.0–2.0 V *vs.* Li/Li^+. This value is rather higher than those of commonly used cathode materials, *e.g.*, $LiCoO_2$ (140 mAh g^{-1}), $LiMn_2O_4$ (148 mAh g^{-1}) and $LiFePO_4$ (170 mAh g^{-1}). Moreover, converting V_2O_5 to hydrated vanadium pentoxide ($V_2O_5{\cdot}xH_2O$) can lead to higher Li-ion storage capacities[7–9] due to its unique crystal structure, which consists of a double layer of V_2O_5 stacked along the *c*-axis of a monoclinic unit cell with water molecules intercalated between the layers.[10] These water molecules expand the distance between the layers, and hence increase the Li-ion-intercalation capacities. For example, a specific energy of over 700 Wh Kg^{-1} has been achieved for Li-ion batteries with a $V_2O_5{\cdot}xH_2O$ xerogel positive electrode.[7]

The cathode application of V_2O_5 is limited by its low diffusion coefficient of Li^+ (~10^{-12} cm^2 s^{-1})[11] and moderate electrical conductivities (10^{-2} to 10^{-3} S cm^{-1}).[12] Many studies have been conducted to improve its lithium diffusion and electrical conductivity by modifying the crystal structure towards a more

[a]*School of Materials Science and Engineering, Nanyang Technological University, 639798, Singapore. E-mail: alexyan@ntu.edu.sg*
[b]*School of Civil and Environmental Engineering, Nanyang Technological University, 639798, Singapore. E-mail: tmlim@ntu.edu.sg*
[c]*Energy Research Institute, Nanyang Technological University, 637459, Singapore*
[d]*School of Life Sciences and Chemical Technology, Ngee Ann Polytechnic, 599489, Singapore*
[e]*TUM CREATE Centre for Electromobility, Nanyang Technological University, 637459, Singapore*

† Electronic supplementary information (ESI) available: TGA curve of HVO; yields and FESEM images of products with different $NH_4H_2PO_4$ concentrations; a digital photograph of the bulky paper made from the mixing of HVO nanobelts and MWCNTs for electrochemical characterization and corresponding FESEM images; a comparative table of our results to other reported V_2O_5 based electrodes. See DOI: 10.1039/c1ra00281c

open framework[13] and by adding conductive coatings.[6] In particular, nanostructured materials are considered as a promising approach to solve these problems by decreasing the polarization and shortening diffusion paths of Li ions.[6,14] Among the nanostructured materials, one-dimensional (1D) nanowires or nanobelts are the most favorable to construct high-performance Li-ion batteries as they can offer a range of unique advantages over their traditional counterparts including large specific surface area, short Li^+ transport distance, efficient 1D electron transport pathways and facile strain relaxation upon electrochemical cycling.[14,15–18] For example, an electrode platform was developed[16] in which silicon nanowires grew directly on the current collector to accommodate the large volume change and to avoid capacity fading. Numerous authors have reported the synthesis of V_2O_5 nanowires/nanobelts by using vapor transport,[19] electrospinning,[15] electrodeposition[20] and hydrothermal approach.[21–23] Some of these methods, however, may only be suitable for small scale sample preparation,[15,19,20] while others may require long synthesis times of about 4–7 days,[21,22] and insulating surface capping such as soft template poly(ethylene oxide).[22] For cathode performance evaluation, it was reported[21] that V_2O_5 nanowires delivered an initial discharge capacity of 351 mAh g^{-1} in the enlarged voltage range of 4.0–1.5 V (corresponding to three Li^+ insertion/extraction) at a current density of 50 mA g^{-1}, which degraded rapidly to 175 mAh g^{-1} after 20 cycles with a capacity retention of 49.9%. Further improvement is desired. On the other hand, fabrication of flexible cathodes using these nanowires/nanobelts has not been demonstrated. Developing binder-free flexible cathodes based on the V_2O_5 1D nanostructure has thus great potential as it can build up flexible Li ion batteries with possibly higher operation temperature ranges and improved Li storage performance. Besides, it also offers the opportunity to explore an energy-saving, low-cost and simple fabrication route to enable large scale production of V_2O_5 nanostructures for practical applications.

Herein, a simple high-yield (close to 100%) hydrothermal approach was developed to prepare single-crystalline hydrated vanadium pentoxide ($V_2O_5{\cdot}0.44H_2O$) nanobelts having a length up to several hundred micrometers and a diameter of only $\sim$20 nm. These $V_2O_5{\cdot}0.44H_2O$ (hereafter abbreviated as HVO) nanobelts were further used to prepare bulky papers without addition of any binders, which were mechanically strong upon bending. The HVO bulky paper was formed by the intertwining HVO nanobelts, which created hierarchical porous channels and facilitated the strain relaxation during the charge and discharge processes. The electrochemical tests revealed that the flexible HVO cathode could deliver high reversible specific capacities, especially at high C rates such as capacity of 163 mAh g^{-1} at 2000 mA g^{-1} (6.8 C).

Experimental

Preparation of HVO nanobelts and bulky paper

In a typical synthesis, 1 mM V_2O_5 powder (Alfa Aesar) and 30 mL H_2O were mixed under vigorous magnetic stirring at room temperature, and then 5 mL of 31% H_2O_2 was added and kept continuously stirred for about 20 min to give a yellow solution. Then, 1.5 mM ammonium dihydrogen phosphate ($NH_4H_2PO_4$, Sigma-Aldrich) was dissolved in the above solution. The resulting solution was transferred to a 50 mL autoclave and kept in an oven at 180 °C for 48 h. The product was washed and separated by centrifugation-redispersion cycles with distilled water and ethanol and then dried at 70 °C to give a yield of $\sim$99% (*i.e.* $\sim$180 mg).

To fabricate the bulky paper, half of the product (90 mg) was redispersed in 40 mL of ethanol solution under vigorous magnetic stirring for about 8 h. The solution was then poured into a petri dish (100×20 mm) with a weighing paper at the bottom and dried in an oven at 70 °C under normal pressure. After the evaporation of ethanol, a flexible yellow HVO bulky paper was easily obtained by peeling it off from the weighing paper.

Chemical physical characterization

X-ray powder diffraction (XRD) was recorded on a Bruker AXS D8 advance X-ray diffractometer at the 2θ range of 10 to 50° using Cu Kα radiation. The morphology was investigated by using a field-emission scanning electron microscopy (FESEM) system (JEOL, Model JSM-7600F), and the nanostructure was characterized by using a transmission electron microscopy (TEM) system (JEOL, Model JEM-2100) operating at 200 kV. Thermogravimetric analysis (TGA, Q500) was carried out from room temperature to 500 °C at a heating rate of 10 K min^{-1} in air. Theta Probe X-ray photoelectron spectroscopy (XPS, ESCALab 250i-XL & Thetaprobe A1333) was used to verify the valence state of vanadium.

Electrochemical characterization

The coin-type cells were assembled in an argon-filled glove-box, where both moisture and oxygen levels were less than 1 ppm. To improve electrical conductivity, a bulky paper with a mixture of 90 mg HVO nanobelts and 30 mg acid-treated multi-walled carbon nanotubes (MWCNTs, C nano) was prepared. The fabrication process was the same as pure HVO paper. Cathodes were made by punching the bulky paper into small disks (Ø = 14 mm), and then pressing upon the stainless steel sheets. For comparative studies, another HVO electrode was prepared by mixing of HVO nanobelts, MWCNTs and poly(vinyldifluoride) (PVDF) at a weight ratio of 75 : 25 : 20 in N-methylpyrrolidone (NMP) solvent and then pasting on the stainless steel sheets. The weight of all active materials was around 2.0 mg. The lithium foils were used as anodes and the electrolyte was a solution of 1 M $LiPF_6$ in ethylene carbonate (EC)/dimethyl carbonate (DMC) (1 : 1, w/w). The cells were tested on a NEWARE multi-channel battery test system with galvanostatic charge and discharge in the voltage range of 4.0–2.0 V. Cyclic voltammetry (scan rate: 0.2 mV s^{-1}) and electrochemical impedance spectra (frequency range: 0.001 $\sim$ 10^5 Hz) were performed with an electrochemical workstation (CHI 660C).

Results and discussion

The phase purity and crystal structure of the product obtained in the presence of 1.5 mM $NH_4H_2PO_4$ was examined by X-ray diffraction (XRD). Fig. 1a reveals that reflection peaks are indexed to the monoclinic $V_2O_5{\cdot}xH_2O$ (JCPDS 07-0332), which is similar to the previous report.[23] To determine the content of

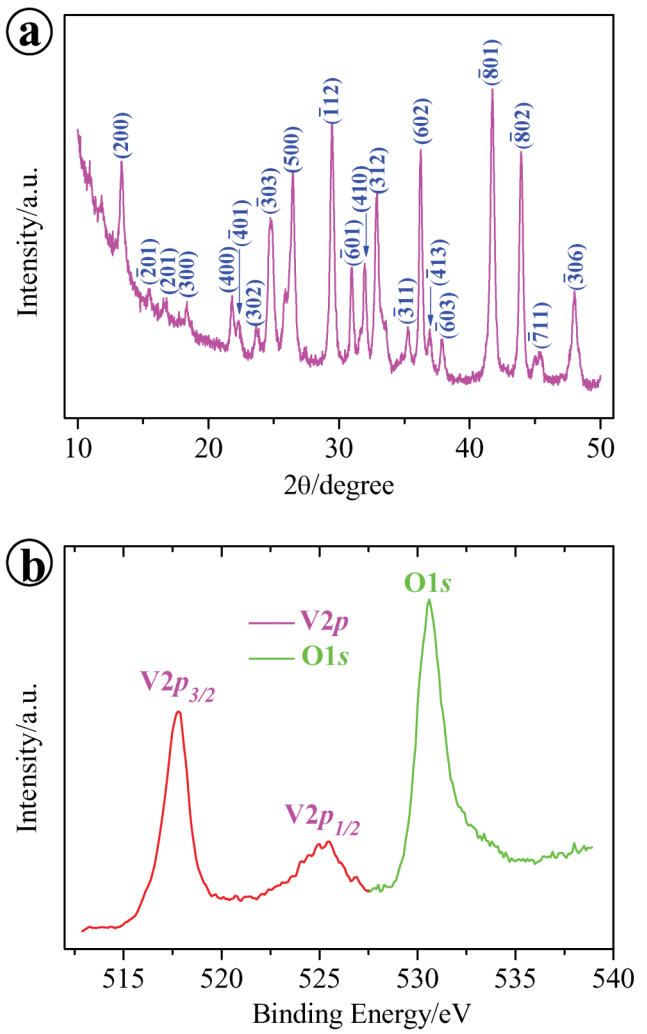

Fig. 1 (a) The XRD pattern of the sample obtained in the presence of 1.5 mM $NH_4H_2PO_4$ and (b) the corresponding XPS spectra for the O 1s and V 2p bands.

coordinated water in the sample, thermogravimetric analysis (TGA) was carried out in air (see ESI, Fig. S1)†. The weight loss of 4.3% below 200 °C is attributed to the release of free water and physically adsorbed water, and the 4.0% weight loss in the temperature range of 200–400 °C is ascribed to the loss of coordinated water in the sample. Thus, the molar ratio of the coordinated water to V_2O_5 is determined to be ~0.44. To further confirm the oxidation state of vanadium, X-ray photoelectron spectroscopy (XPS) analysis was also carried out on the as-prepared sample (see Fig. 1b). The V $2p_{3/2}$ band at 517.7 eV and the O 1s band at 530.6 eV correspond to the V(5+)-O stretch, which agrees well with the previous report.[24]

The field emission scanning electron microscopy (FESEM) images shows that the as-prepared sample is a 1D nanostructure (see Fig. 2a–b) with a length of 100–400 μm. The transmission electron microscopy (TEM) image (see Fig. 2c) reveals that the as-prepared HVO is a nanobelt structure with a width in the range of 20–600 nm. As some of the HVO can be rolled up to provide the side view of the nanobelts (see Fig. 2d), the thickness of the nanobelts is estimated to be around 10 nm. Here, it is noted that the width of the HVO nanobelts determined through TEM is much smaller than that observed in the FESEM, due to the fact that FESEM images mainly show bundles of HVO nanobelts. The high resolution (HR) TEM image (see Fig. 2e) and the selected area electron diffraction (SAED) pattern (see inset of Fig. 2e) indicated that these nanobelts are single crystalline. The HRTEM observation also indicates that the long axis of the nanobelts is oriented along [010] direction with the observed interfringe spacing of 0.67 nm and this corresponds well to the (200) planes of monoclinic HVO (JCPDS 07-0332). It is noted that the (200) lattice spacing of HVO is larger than that of crystalline V_2O_5 (*e.g.* 0.58 nm),[25] which may facilitate lithium intercalation.

The growth of 1D HVO nanobelts is attributed to the anisotropic bonding of its layered structure resulting in selected growth. The [010] or *b*-axis is the fastest growth direction and [001] is the slowest due to the weak *c*-axis bonding.[17] Moreover, in our reaction system, the presence of $NH_4H_2PO_4$ (hereafter abbreviated as ADP) during the synthesis is noted to affect the yield of HVO products (see ESI, Fig. S2)† and the sample morphology (see ESI, Fig. S3)†. Here, the yield of the products is determined by the weight percentage of dried products to the V_2O_5 reactant. It is found that the product yield is only ~0.2% without ADP during the synthesis. The yield of products increases to ~78.6% and ~99.0% when ADP is added at concentration (I_{ADP}) of 0.5 mM and 1.5 mM, respectively. Further increase in ADP concentration does not show significant change. FESEM images of the HVO nanobelts prepared under different I_{ADP} values reveal that increasing I_{ADP} from 0 to 1.5 mM does not show obvious changes in morphology and nanostructure (see ESI, Fig. S3a–c)†, however nanorods are observed when I_{ADP} is increased to 2.0 mM (see ESI, Fig. S3d)† with shorter length, *e.g.* 10–50 μm, and larger width, *e.g.* 50–100 nm.

The HVOs products are further used to fabricate the bulky paper as per described in the experimental section. The bulky papers prepared from the long nanobelts synthesized with appropriate amount of ADP (0.5~1.5 mM) are robust upon bending and a representative one is shown in Fig. 2f, while the bulky paper prepared with HVO nanorods is fragile and easily broken upon bending, which is probably due to that the shorter nanorods can not form intertwining networks. For Li ion battery cathode applications, HVO nanobelts were chose as the electrode materials and were further mixed with 25 wt% acid-treated multi-walled carbon nanotubes (MWCNTs) to make flexible battery electrodes (see ESI, Fig. S4a)†, to make it mechanically stronger than the acetylene black. The FESEM images (see ESI, Fig. S4c–d)† indicate uniform mixture of the MWCNTs and HVO nanobelts in the bulky paper electrodes. The thickness of the bulky-paper cathodes was controlled around ~50 μm.

To study the Li-ion storage properties of binder-free bulky paper cathodes made from HVO nanobelts, a series of electrochemical measurements were carried out based on the half cell configuration.[26–28] Fig. 3a depicts representative cyclic voltammograms (CVs) of the HVO electrodes for the first three cycles at a scan rate of 0.2 mV s^{-1} in the voltage range of 4.0 to 2.0 V. The CVs exhibited two pairs of reduction and oxidation peaks associated with the phase transitions of HVO during Li^+ intercalation and deintercalation processes. The two reduction peaks located at ~2.84 and ~2.47 V, respectively, are attributed to the reduction of V^{5+} to V^{4+} through the reaction of

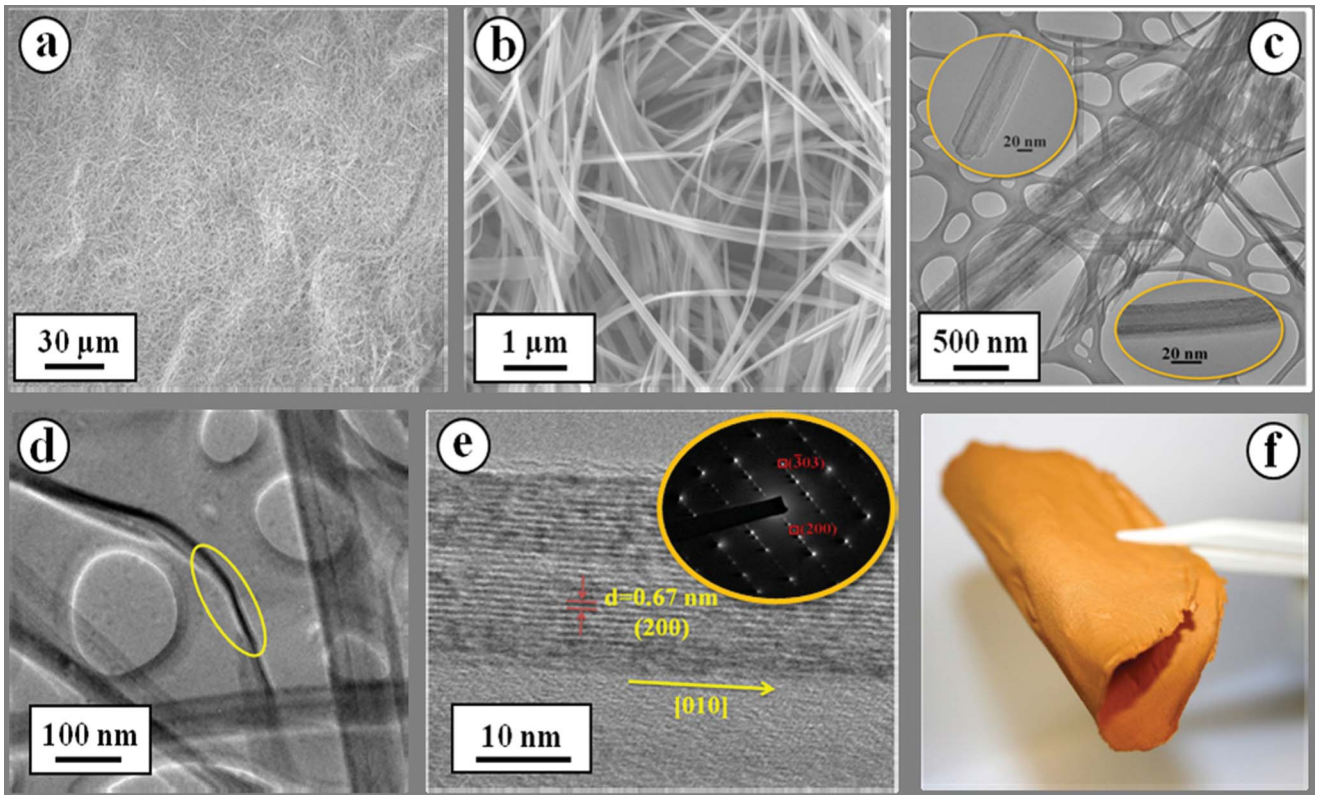

Fig. 2 (a) Low- and (b) high-magnification FESEM images of HVO nanobelts. (c) TEM image of nanobelts. The inset in (c) is a magnified view to show the width of the nanobelts. (d) Side view of a rolled up nanobelt giving a thickness of ~10 nm. (e) HRTEM image of an individual nanobelt with its corresponding SAED pattern (inset). (f) Optical image of a freestanding HVO bulky paper based on the intertwining network of above HVO nanobelts without addition of any binders.

$V_2O_5{\cdot}0.44H_2O + xLi^+ + xe^- \rightarrow Li_xV_2O_5{\cdot}0.44H_2O$, where x is around 2. The reverse reactions are then indicated by the two corresponding oxidation peaks at around 2.70 and 2.94 V. The symmetrical feature of the CV curves suggests a good reversibility of the cycling processes. Fig. 3b exhibits galvanostatic charge-discharge voltage profiles of the HVO nanobelts electrode between 2.0 and 4.0 V at a current density of 50 mA g^{-1} (0.17 C). The obscure potential plateaus observed in the charge-discharge curves are consistent with redox peaks in the CV curves. In addition, the symmetrical characteristic of potential plateaus in the charge and discharge profiles suggests the highly reversible phase transition processes. The insertion process gives an initial discharge capacity of 297 mAh g^{-1} and a subsequent charge capacity of 297 mAh g^{-1} with no irreversible capacity loss. Although slightly decreased, the reversible discharge capacity still can reach 231 mAh g^{-1} during the 20th cycle with the Coulombic efficiency consistently being maintained at ~100%. This cycling performance is better than those previously reported for V_2O_5[29,30] and $V_2O_5{\cdot}xH_2O$[23] cathodes.

The cycling responses of the HVO bulky-paper electrode at different C rates were evaluated and shown in Fig. 3c. The electrode shows a high discharge capacity of 283 mAh g^{-1} during the 2nd cycle at a current density of 100 mA g^{-1} (0.34 C) and subsequently reduces to 241, 212, 194 and 183 mAh g^{-1} at current densities of 200 (0.68 C), 500 (1.7 C), 800 (2.7 C) and 1000 mA g^{-1} (3.4 C), respectively. Even at a high current density of 2000 mA g^{-1} (6.8 C), the HVO binder-free bulky-paper electrode can still deliver a high capacity of 163 mAh g^{-1} during the 2nd cycle. For comparative studies, another HVO electrode was prepared by conventional tap-casting process with 17 wt% polyvinylidene fluoride (PVDF). It is found that the HVO nanobelts cathode with PVDF binder exhibits an inferior performance (see Fig. 3c), giving discharge capacities of 271, 219, 193, 178, 168 and 143 mAh g^{-1} during the 2nd cycle at current densities of 200 (0.68 C), 500 (1.7 C), 800 (2.7 C), 1000 (3.4 C) and 2000 mA g^{-1} (6.8 C), respectively. The inferior Li storage properties of PVDF-added HVO cathodes is mainly attributed to their low electrical conductivity as verified by the electrochemical impedance spectra (see Fig. 3d). The PVDF-added HVO cathodes shows a larger radius of semi-circle in the Nyquist plots compare to that of the binder-free HVO electrodes, and thus indicates higher charge-transfer resistance. As compare to V_2O_5 based electrodes prepared by other reported processes,[29,31–33] the above demonstrated Li storage performance of HVO bulk paper electrode is outstanding (see ESI, Table S1)†. There are reports on achieving high discharge capacities for nanostructured V_2O_5 electrodes.[32–34] For example, nano-sized V_2O_5[32] showed a 2nd-cycle discharge capacity of 148 mAh g^{-1} at a current density of 2352 mA g^{-1}; V_2O_5 nanobelt arrays grew on a Ti substrate[33] depicted a 2nd-cycle discharge capacity of 192 mAh g^{-1} at 1000 mA g^{-1}; V_2O_5/carbon tube-in-tube (CTIT) nanocomposites[34] delivered a 2nd-cycle discharge capacity of 200 mAh g^{-1} at 2352 mA g^{-1}. However, it is worth pointing out that the higher performances reported by others are achieved in thin film V_2O_5 electrodes (2.5–3 μm thickness[33]) while this paper reports on thick films of ~50 μm. For evaluation of the effective energy density of

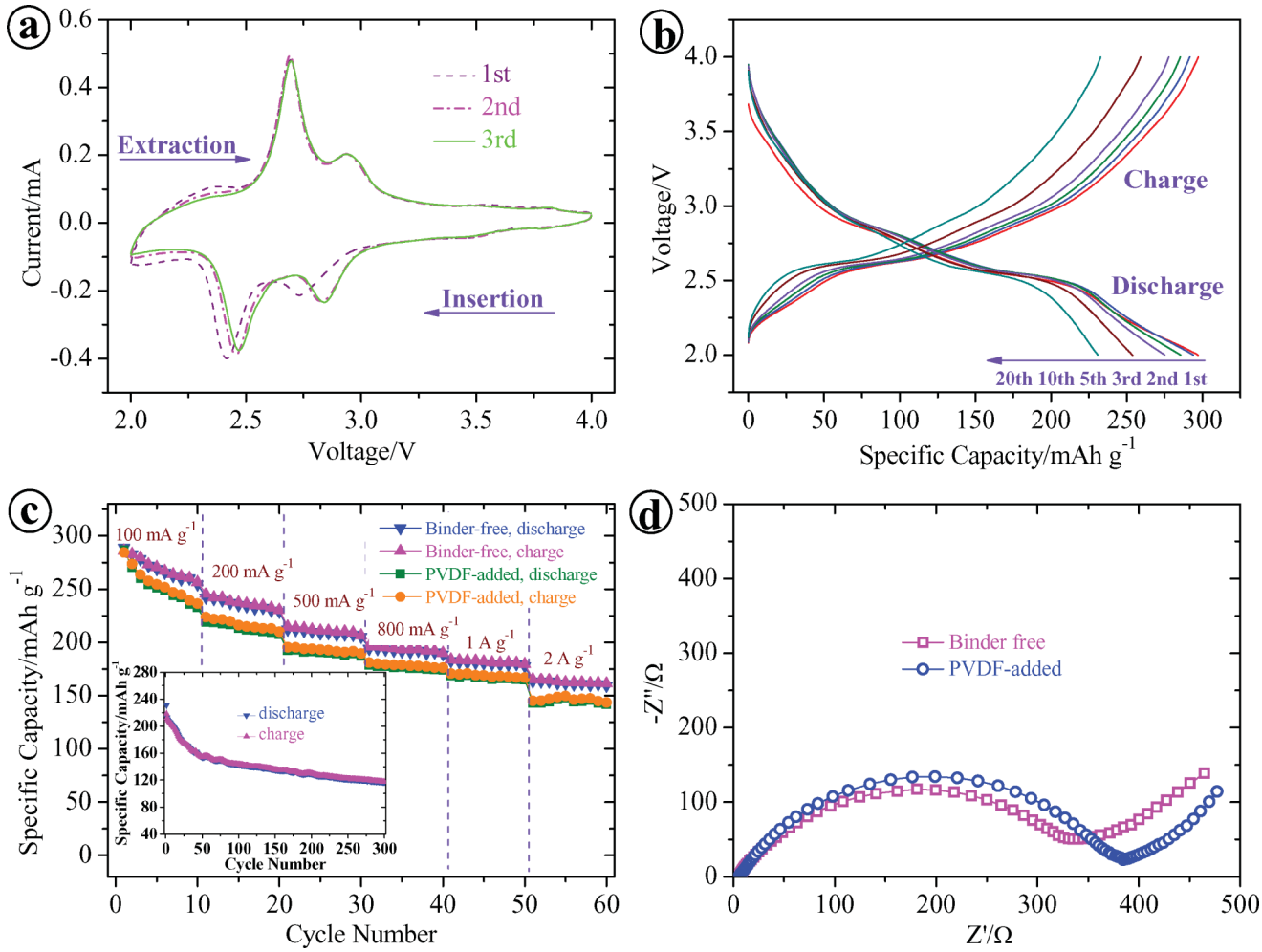

Fig. 3 Cathode performance of binder-free bulky paper made from HVO nanobelts in the voltage range of 4.0–2.0 V. (a) CV curves of the first three cycles at a scan rate of 0.2 mV s^{-1}. (b) Galvanostatic charge-discharge voltage profiles at a current density of 50 mA g^{-1}. (c) A comparison of charge/discharge capacities of binder-free bulky paper electrode and PVDF-added HVO electrode at various current densities of 100 to 2000 mA g^{-1}. Here, the PVDF was not counted into the active material weight. Inset in (c): cycling performance of binder-free HVO bulky paper electrode at a high current density of 2000 mA g^{-1}. (d) Electrochemical impedance spectra of above two electrodes measured at the 4th fully discharged state. The high-middle frequency semicircle represents the charge-transfer process and a straight slopping line at low frequencies corresponds to Li^+ diffusion in HVO electrode known as Warburg impedance.

the full battery cell, the average weight of current collectors and other inactive components will be added in. Thin film electrodes then will result in low effective energy densities. Moreover, our HVO bulky-paper electrode exhibits an excellent cyclability at a high current density of 2000 mA g^{-1} (6.8 C) as shown in the inset of Fig. 3c, delivering a discharge capacity of 118 mAh g^{-1} during the 300th cycle. Such high-C-rate performance is better than other well-reported cathodes, *e.g.* spinel $LiMn_2O_4$ nanorods[35] showed a capacity of 85 mAh g^{-1} during the 100th cycle at 1 C rate and flowerlike $LiFePO_4$/C microspheres[36] delivered a stable capacity of 85 mAh g^{-1} during the 400th cycle at 5C rate. The superior performance of HVO flexible electrodes is believed to result from the following aspects: (1) the 10-nm thick HVO nanobelts with large specific surface area provide efficient electron transport pathways and short diffusion distances for Li^+ intercalation/deintercalation; (2) the binder-free preparation process of the electrodes increases their electrical conductivity; (3) the hierarchical porous channels in the intertwining network of HVO nanobelts relax the mechanical strain generated upon the charge-discharge cycling.

Conclusions

We have developed a simple hydrothermal approach to prepare HVO nanobelts with high production yield up to ~99%. Flexible bulky-paper cathodes without addition of any binder are prepared using these HVO nanobelts. These flexible electrodes show high reversible Li storage capacities, good high C-rate performance with ~100% coulombic efficiency. These promising properties of binder-free flexible electrodes can be an important step for development of rollable rechargeable battery with desired energy storage performance.

Acknowledgements

The authors gratefully acknowledge AcRF Tier 1 RG 31/08 of MOE (Singapore), NRF2009EWT-CERP001-026 (Singapore),

Singapore Ministry of Education (MOE2010-T2-1-017), A*STAR SERC grant 1021700144 and Singapore MPA 23/04.15.03 grant. H.Z. thanks MOE2010-T2-1-060) from MOE in Singapore and the New Initiative fund FY 2010 (M58120031) from NTU, Singapore.

References

1 B. J. Landi, M. J. Ganter, C. D. Cress, R. A. DiLeo and R. P. Raffaelle, *Energy Environ. Sci.*, 2009, **2**, 638–654.
2 S. Y. Chew, S. H. Ng, J. Z. Wang, P. Novak, F. Krumeich, S. L. Chou, J. Chen and H. K. Liu, *Carbon*, 2009, **47**, 2976–2983.
3 C. Y. Wang, D. Li, C. O. Too and G. G. Wallace, *Chem. Mater.*, 2009, **21**, 2604–2606.
4 J. Liu, H. Xia, D. F. Xue and L. Lu, *J. Am. Chem. Soc.*, 2009, **131**, 12086–12087.
5 D. M. Yu, S. T. Zhang, D. W. Liu, X. Y. Zhou, S. H. Xie, Q. F. Zhang, Y. Y. Liu and G. Z. Cao, *J. Mater. Chem.*, 2010, **20**, 10841–10846.
6 H. Yamada, K. Tagawa, M. Komatsu, I. Moriguchi and T. Kudo, *J. Phys. Chem. C*, 2007, **111**, 8397–8402.
7 K. West, B. Zachauchristiansen, T. Jacobsen and S. Skaarup, *Electrochim. Acta*, 1993, **38**, 1215–1220.
8 C. C. Torardi, C. R. Miao, M. E. Lewittes and Z. Li, *J. Solid State Chem.*, 2002, **163**, 93–99.
9 D. W. Liu, Y. Y. Liu, B. B. Garcia, Q. F. Zhang, A. Q. Pan, Y. H. Jeong and G. Z. Cao, *J. Mater. Chem.*, 2009, **19**, 8789–8795.
10 V. Petkov, P. N. Trikalitis, E. S. Bozin, S. J. L. Billinge, T. Vogt and M. G. Kanatzidis, *J. Am. Chem. Soc.*, 2002, **124**, 10157–10162.
11 T. Watanabe, Y. Ikeda, T. Ono, M. Hibino, M. Hosoda, K. Sakai and T. Kudo, *Solid State Ionics*, 2002, **151**, 313–320.
12 J. Muster, G. T. Kim, V. Krstic, J. G. Park, Y. W. Park, S. Roth and M. Burghard, *Adv. Mater.*, 2000, **12**, 420–424.
13 M. Hibino, M. Ugaji, A. Kishimoto and T. Kudo, *Solid State Ionics*, 1995, **79**, 239–244.
14 Y. Wang and G. Z. Cao, *Chem. Mater.*, 2006, **18**, 2787–2804.
15 L. Q. Mai, L. Xu, C. H. Han, Y. Z. Luo, S. Y. Zhao and Y. L. Zhao, *Nano Lett.*, 2010, **10**, 4750–4755.
16 C. K. Chan, H. L. Peng, G. Liu, K. McIlwrath, X. F. Zhang, R. A. Huggins and Y. Cui, *Nat. Nanotechnol.*, 2008, **3**, 31–35.
17 C. K. Chan, H. L. Peng, R. D. Twesten, K. Jarausch, X. F. Zhang and Y. Cui, *Nano Lett.*, 2007, **7**, 490–495.
18 R. Liu, J. Duay and S. B. Lee, *Chem. Commun.*, 2011, **47**, 1384–1404.
19 M. C. Wu and C. S. Lee, *J. Solid State Chem.*, 2009, **182**, 2285–2289.
20 C. C. Hu, K. H. Chang, C. M. Huang and J. M. Li, *J. Electrochem. Soc.*, 2009, **156**, D485–D489.
21 T.Y. Zhai, H. M. Liu, H. Q. Li, X. S. Fang, M. Y. Liao, L. Li, H. S. Zhou, Y. Koide, Y. Bando and D. Goberg, *Adv. Mater.*, 2010, **22**, 2547–2552.
22 C. V. S. Reddy, J. Wei, Z. Quan-Yao, D. Zhi-Rong, C. Wen, S. Mho and R. R. Kalluru, *J. Power Sources*, 2007, **166**, 244–249.
23 B. X. Li, Y. Xu, G. X. Rong, M. Jing and Y. Xie, *Nanotechnology*, 2006, **17**, 2560–2566.
24 G. Silversmit, D. Depla, H. Poelman, G. B. Marin and R. De Gryse, *J. Electron Spectrosc. Relat. Phenom.*, 2004, **135**, 167–175.
25 S. L. Chou, J. Z. Wang, J. Z. Sun, D. Wexler, M. Forsyth, H. K. Liu, D. R. MacFarlane and S. X. Dou, *Chem. Mater.*, 2008, **20**, 7044–7051.
26 J. X. Zhu, Z. Y. Lu, M. O. Oo, H. H. Hng, J. Ma, H. Zhang and Q. Y. Yan, *J. Mater. Chem.*, 2011, DOI: 10.1039/c1jm12447a.
27 J. X. Zhu, T. Zhu, X. Z. Zhou, Y. Y. Zhang, X. W. Lou, X. D. Chen, H. Zhang, H. H. Hng and Q. Y. Yan, *Nanoscale*, 2011, **3**, 1084–1089.
28 S. Saadat, Y. Y. Tay, J. X. Zhu, P. F. Teh, S. Maleksaeedi, M. M. Shahjamali, M. Shakerzadeh, M. Srinivasan, B. Y. Tay, H. H. Hng, J. Ma and Q. Y. Yan, *Chem. Mater.*, 2011, **23**, 1032–1038.
29 Y. Chen, H. Liu and W. L. Ye, *Scr. Mater.*, 2008, **59**, 372–375.
30 C. Q. Feng, S. Y. Wang, R. Zeng, Z. P. Guo, K. Konstantinov and H. K. Liu, *J. Power Sources*, 2008, **184**, 485–488.
31 S. Q. Wang, D. Wang, C. G. Li, C. H. Chen and Y. D. Yin, *J. Mater. Chem.*, 2011, **21**, 6365–6369.
32 A. Q. Pan, J. G. Zhang, Z. M. Nie, G. Z. Cao, B. W. Arey, G. S. Li, S. Q. Liang and J. Liu, *J. Mater. Chem.*, 2010, **20**, 9193–9199.
33 Y. Wang, H. J. Zhang, W. X. Lim, J. Y. Lin and C. C. Wong, *J. Mater. Chem.*, 2011, **21**, 2362–2368.
34 Y. S. Hu, X. Liu, J. O. Muller, R. Schlogl, J. Maier and D. S. Su, *Angew. Chem., Int. Ed.*, 2009, **48**, 210–214.
35 D. K. Kim, P. Muralidharan, H. W. Lee, R. Ruffo, Y. Yang, C. K. Chan, H. Peng, R. A. Huggins and Y. Cui, *Nano Lett.*, 2008, **8**, 3948–3952.
36 C. W. Sun, S. Rajasekhara, J. B. Goodenough and F. Zhou, *J. Am. Chem. Soc.*, 2011, **133**, 2132–2135.